Bicircular attoclock with molecules as a probe of strong-field Stark shifts and molecular properties

Paul Winter ⬤ and Manfred Lein ⬤[*]

Leibniz University Hannover, Institute of Theoretical Physics, Appelstraße 2, 30167 Hannover, Germany

A theoretical study of the orientation-dependent attoclock shift in photoelectron momentum distributions generated by ionization of HeH$^+$ by a counter-rotating two-color bicircular laser field is presented. Solutions of the two-dimensional time-dependent Schrödinger equation are extrapolated to the adiabatic limit and compared to two-step trajectory models. The trajectory models are sensitive to the choice of the tunnel exit point, which depends on the dipole moment and polarizability tensor of the molecule. Using a suitable trajectory model, we are thus able to reconstruct these molecular properties from the momentum distributions within about 7% deviation from the exact values.

Introduction. Strong-field ionization is the foundation of important light-matter interaction phenomena in atoms and molecules such as high-harmonic generation [1], laser-induced electron diffraction [2–6], and strong-field photoelectron holography [7–9]. Molecules are more complex than atoms and they give us the possibility to study how the ionization process depends on the electronic and geometric structure of the target system. The electron dynamics crucially depends on properties such as the nodal structure or symmetry of the highest occupied molecular orbital [10,11]. Further, the interaction with the light field changes the ionization potential of the molecule via the Stark effect. Molecular properties such as the dipole moment and the polarizability tensor lead to a dependence of the ionization dynamics on the molecular orientation, which has to be considered for the proper modeling of experiments [12–16]. In this article, we concentrate specifically on molecular ionization in the adiabatic limit defined by a small Keldysh parameter, $\gamma = \omega\sqrt{2I_p}/E$, with the ionization potential I_p, the electric field-strength amplitude E, and the frequency ω. A small Keldysh parameter $\gamma \ll 1$ places the interaction into the tunneling regime of strong-field ionization [17].

For the study of strong-field ionization, a very successful experimental setup is the attosecond angular streaking, the "attoclock." It provides a mapping between the time of ionization and the final momentum of the ejected electron [18–29]. Measuring the photoelectron momentum distribution (PMD) is therefore a rich source for time-resolved investigations of the ionization step [30–35]. Typical implementations are based on close-to-circularly polarized light fields. However, for observables that depend on molecular orientation, deconvolution methods must be used to extract the information of interest from the angle-dependent signal, introducing potential uncertainties [26,27]. One alternative could be the quasilinear bicircular attoclock [36,37], which uses a counter-rotating two-color bicircular ω-2ω light field [38–42] with the

relative strength of the two colors adjusted such that the electric field is nearly linearly polarized in a time window around the maximal field strength. This light field combines the properties of the attoclock setup (time-to-momentum mapping) with the benefits of linear polarization (sharp field direction at the time of ionization). Due to the exponential dependence of the ionization rate on the field strength in strong-field ionization [43], the quasilinear field can eliminate the need for deconvolution. Conventional linearly polarized fields involve rescattering of the freed electron with the core, leading to complicated structures in the PMD and making the analysis of the orientation dependence more difficult. The bicircular attoclock, on the other hand, avoids rescattering and promises an easier interpretation compared to linear polarization.

Trajectory-based models are often used to interpret the PMDs. In such a model, the production of a photoelectron consists of (i) the ionization step and (ii) classical propagation of the freed electron. In the first step, the electron appears in the vicinity of the parent ion after tunneling through the barrier created from the molecular potential and the instantaneous electric field. A variety of different exit-point models are out there [44] and it is an open question which one is the best choice in the adiabatic limit, particularly for molecules. In the second step the electron moves on a classical trajectory in the combined potential of the parent ion and the light field. The simplest possible trajectory model is the "simple man's model" [45], where the Coulomb force of the residual ion is fully neglected. In this case, the electron's final momentum equals the negative vector potential $-\vec{A}(t_0)$ of the light field at the time t_0 of ionization. This gives us a natural reference to compare with when studying the effect of the Coulomb potential in the ionization process. Tunnel ionization in parabolic coordinates with induced dipole and Stark shift (TIPIS) [46] is a widely used model for the exit point, based on adiabatic assumptions about the tunneling process such as zero initial velocity and maximal ionization at the moment of maximal field strength [25,37,47]. For a pure Coulomb potential, the TIPIS model exploits the separation of the stationary Schrödinger equation in parabolic

---

[*]lein@itp.uni-hannover.de

coordinates, leading to a well-defined one-dimensional tunneling picture. For molecules, this assumption can be fulfilled only approximately. Hence, there is a need to use time-dependent Schrödinger equation (TDSE) solutions to validate the TIPIS model for molecules. Alternatives are the field-direction model (FDM), assuming a one-dimensional picture of tunneling along the direction defined by the instantaneous field [48], and the triangular-barrier width (TBW) I_p/E [17]. In this article, all of them are compared with TDSE solutions in the adiabatic limit. We then show that the TIPIS model can be used to extract orientation-dependent molecular properties from strong-field photoelectron momentum distributions.

Numerical model. We solve the two-dimensional single-active-electron TDSE in dipole approximation with fixed nuclei on a Cartesian grid (at least 2048×2048 points and 300×300 a.u.) using the split-operator method [49] with a time step of $\Delta t = 0.006$ a.u. The potential

$$V(\vec{r}) = \frac{-1}{\sqrt{(\vec{r} - \vec{r}_1)^2 + \alpha_1}} + \frac{-(1 + e^{-\beta(\vec{r} - \vec{r}_2)^2})}{\sqrt{(\vec{r} - \vec{r}_2)^2 + \alpha_2}}, \quad (1)$$

with $\beta = 1.063$ a.u., $\alpha_1 = \alpha_2 = 0.5$, and an internuclear distance of $R = |\vec{r}_1 - \vec{r}_2| = 1.4$ a.u. is used to represent the HeH$^+$ molecule (H at $\vec{r}_1$ and He at $\vec{r}_2$). On the specified grid, this potential results in an ionization potential of $I_p \approx 1.657$ a.u. The ground state is calculated with imaginary-time propagation [50], followed by the real-time propagator eigenstate method [51]. The outgoing wave packet is projected onto Volkov states using an absorbing potential [52]. To ensure a smooth transition, the core potential is damped to zero within 30 a.u. before the absorber starts. The counter-rotating bicircular field is described by the vector potential

$$\vec{A}(t) = \frac{-1}{\sqrt{1 + \varepsilon^2}} \frac{E_0}{\omega} f(t) \left[\begin{pmatrix} \cos(\omega t) \\ \sin(\omega t) \end{pmatrix} + \frac{\varepsilon}{2} \begin{pmatrix} -\cos(2\omega t) \\ \sin(2\omega t) \end{pmatrix} \right], \quad (2)$$

where ε is the ratio of the second harmonic to the fundamental harmonic component of the electric field $\vec{E}(t) = -\partial_t \vec{A}(t)$. The maximal electric field strength is reached at $t = 0$ and it is given by

$$E_{\text{peak}} = E_0 \frac{1 + \varepsilon}{\sqrt{1 + \varepsilon^2}}. \quad (3)$$

For a cw field with $f(t) \equiv 1$, the choice $\varepsilon = 1/2$ leads to a quasilinear behavior [37] in the vicinity of $t = 0$, where

$$\vec{A}_{\text{eff}}(t) = A_x(0)\vec{e}_x - E_{\text{peak}}/\omega_{\text{eff}} \sin(\omega_{\text{eff}} t)\vec{e}_y, \quad (4)$$

$$\vec{E}_{\text{eff}}(t) = E_{\text{peak}} \cos(\omega_{\text{eff}} t)\vec{e}_y, \quad (5)$$

with $\vec{E}(t) = \vec{E}_{\text{eff}}(t) + O(t^3)$ and $\omega_{\text{eff}} = \omega\sqrt{2}$. The time-averaged intensity in this case is $c\epsilon_0 E_0^2$. A nonconstant envelope function $f(t)$, however, disturbs the quasilinear behavior. Nevertheless, one can adjust the ratio ε to ensure again linearity up to $O(t^3)$ in the electric field. The optimal ratio ε_{opt} for the envelope $f(t) = \cos^4(\frac{\omega t}{2N_p})$ used below (with N_p being the number of cycles) is

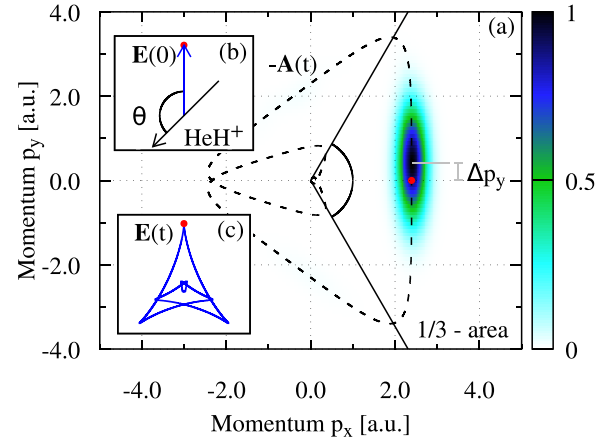$$\varepsilon_{\text{opt}} = \frac{2(1 + N_p^2)}{1 + 4N_p^2}. \quad (6)$$

FIG. 1. (a) Normalized photoelectron momentum distribution from ionization of HeH$^+$ at $\theta = 180°$ (ionization via the H-side) for a frequency ω corresponding to $\lambda = 1131$ nm and $E_0 = 0.15$ a.u. (intensity 1.6×10^{15} W/cm^2). The attoclock shift Δp_y and the 1/3 area used for analysis are indicated. Dashed line: Negative vector potential. (b) Definition of the orientation angle θ. The molecular axis as the black arrow points from He to H. (c) Electric field. The red dot marks $t = 0$.

This is obtained by forcing the quadratic term of the Taylor series of $A_x(t)$ to be zero, $\ddot{A}_x(0) = 0$, so the linear term in $E_x(t)$ vanishes. In the following calculations, we always use $\varepsilon = \varepsilon_{\text{opt}} = 0.\overline{540}$ (corresponding to $N_p = 3$) and $\gamma = \omega_{\text{eff}}\sqrt{2I_p}/E_{\text{peak}}$ to characterize the adiabaticity. After the adjustment of ε, the effective frequency of the quasilinear field is

$$\omega_{\text{eff}} = \omega \sqrt{\frac{8\varepsilon_{\text{opt}}^2 + 13\varepsilon_{\text{opt}} - 4}{2 + \varepsilon_{\text{opt}} - \varepsilon_{\text{opt}}^2}}. \quad (7)$$

Figure 1 shows one example of a photoelectron momentum distribution. The signal at $p_x > 0$ originates from ionization around the time when the field reaches its global maximum [$t = 0$, see red dot in Fig. 1(c)]. Secondary maxima in the PMD corresponding to the lower two peaks in the electric field strength [see Fig. 1(c)] are more suppressed in this example compared to the atomic case [36], so only one major peak is visible on a linear scale. This is due to the orientation-dependent ionization probability of ground-state HeH$^+$ becoming maximal when the field points along the molecular axis such that ionization proceeds over the H side. Rotating the molecule can lead to the appearance of another maximum in the PMD when the molecular axis is parallel to one of the local field maxima. In the following, however, we concentrate on the main maximum (the one appearing in the marked 1/3 area in the right of Fig. 1). This peak is displaced upwards with respect to the prediction of the simple man's model [red dot in Fig. 1(a)] that neglects the Coulomb potential. We refer to this displacement as the attoclock shift Δp_y. This experimentally accessible observable has the advantage of being highly sensitive to orientation-dependent and nonadiabatic effects. We extract the attoclock shift from TDSE simulations by a Gaussian fit to the photoelectron momentum distribution in the close vicinity of the maximum. We define the orientation angle θ as the angle
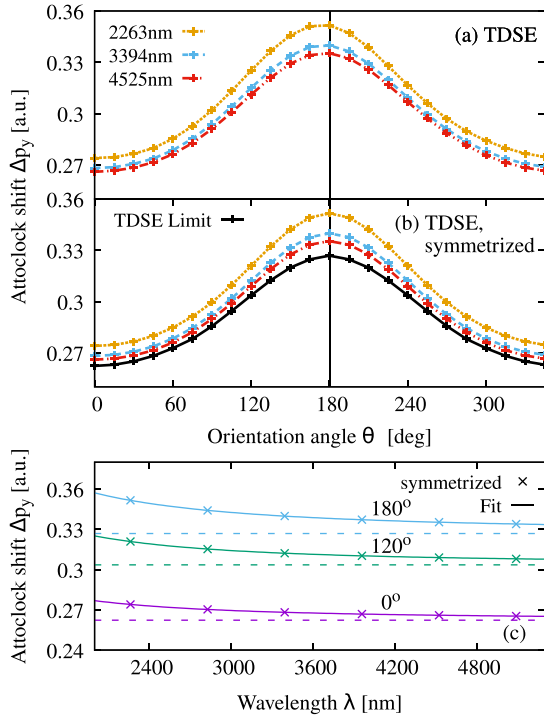
FIG. 2. Orientation-dependent attoclock shift obtained from TDSE solutions for different wavelengths λ and fixed electric field strength $E_0 = 0.15$ a.u. (a) TDSE results. (b) Symmetrized TDSE results with extrapolated adiabatic limit (black). (c) Extrapolation procedure for three orientations: Crosses show the symmetrized TDSE results for different wavelengths; solid lines are the fits; and dashed lines illustrate the adiabatic limit.
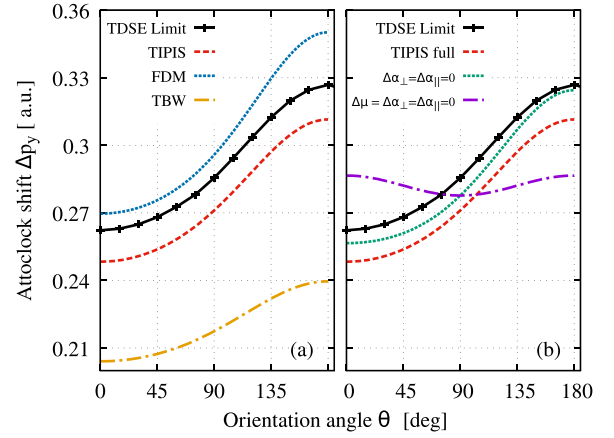

FIG. 3. (a) Symmetrized and extrapolated attoclock shifts from TDSE calculations (black) for $E_0 = 0.15$ a.u. compared to two-step models with different exit points. (b) Comparison with the TIPIS-based two-step model with fewer parameters. The exact molecular parameters (Table I) are used.

between the direction of the maximal electric field (positive y direction) and the molecular axis [vector pointing from the He side to the H side, see Fig. 1(b)]. We rotate the molecule anticlockwise, so $\vec{r}_1 = -\vec{r}_2 = (0, 0.7)^T$ corresponds to $\theta = 0°$ and $\vec{r}_1 = -\vec{r}_2 = (0.7, 0)^T$ corresponds to $\theta = 270°$. The orientation angle is fixed for one simulation of the TDSE. Further, the orientation of the field is the same for all calculations, so the electron tunnels into the negative y direction. Although we use quite long wavelengths, which can potentially cause nondipole effects [53], we neglect them by restricting the simulations to two dimensions and thereby dramatically reduce the computational effort. Nondipole effects mostly lead to shifts in propagation direction. These shifts can be well estimated in perturbation theory [54] and leave the attoclock shift approximately unchanged. Besides the nondipole shift, we do not expect substantial differences compared to three-dimensional simulations. Note that the differences previously seen [55] in the comparison of the two- and three-dimensional results arose from interference of direct and rescattered trajectories, while in the present case, rescattering is absent.

Adiabatic limit. The orientation dependence of Δp_y in Fig. 2(a) shows that the attoclock shift is significantly larger when the electron tunnels via the H side ($\theta = 180°$) compared to tunneling via the He side ($\theta = 0°$). Below, we explain this finding within a trajectory model without invoking any orientation dependence of the dominant ionization time. We notice that the curves exhibit a slight asymmetry with respect to $180°$. Increasing the wavelength reduces the asymmetry, while approaching the quasistatic limit. Importantly, we have found that the asymmetry becomes much larger when a nonoptimized ratio, e.g., $\varepsilon = 1/2$, is used and that this asymmetry increases for longer wavelengths (not shown). This can be explained by a slight shift of the electron release times away from $t = 0$ due to a preferred ionization along the molecular axis [26,27], an effect that occurs only in a small time window around $t = 0$. The optimization of the ratio ε suppresses such a release-time shift, because it minimizes the change of field direction during the time of significant ionization. This is an important benefit of the quasilinear field. As we will discuss elsewhere, extensive classical and TDSE simulations suggest that the small remaining asymmetry in the finite-wavelength TDSE results is not due to the anisotropy of the electron-ion force acting on outgoing trajectories, but it is instead due to nonadiabatic ionization dynamics and it disappears in the long-wavelength limit. Motivated by these observations, we symmetrize the TDSE orientation dependence of the attoclock shift by taking the mean value for each pair of orientations mirrored about $180°$. This leads to the curves in Fig. 2(b). We extrapolate the symmetrized TDSE results for each angle from finite wavelengths to infinity via $\Delta p_y = \Delta p_{\text{Limit}} + \frac{c_1}{\lambda} + \frac{c_2}{\lambda^2}$ [see Fig. 2(c)]. In the previous studies [26,27], only molecules without a permanent dipole were investigated. In that case, the symmetric part of the angle scans is almost a constant function [cf. Fig. 3(b) below]. In contrast, the HeH$^+$ molecule considered here has a strong dipole moment, leading to a substantial angle dependence.

To interpret the TDSE results, we resort to adiabatic trajectory models where we need to choose the exit point of the electron at the time of ionization. In the following, we use the TIPIS model [46], the FDM [48], and the TBW [17] to calculate the exit point. We include a quadratic approximation of the Stark-shifted and orientation-dependent ionization

potential:

$$I_p(E, \theta) = I_p(0) + \Delta\mu \cos(\theta)E$$
$$+ \frac{1}{2}[\Delta\overline{\alpha} + \Delta\alpha_d \cos(2\theta)]E^2 + O(E^3), \quad (8)$$

where $\Delta\mu$ is the dipole moment of the bound-electron orbital and its polarizabilities are given by $\Delta\alpha_{\parallel} = \Delta\overline{\alpha} + \Delta\alpha_d$ and $\Delta\alpha_{\perp} = \Delta\overline{\alpha} - \Delta\alpha_d$ [12–14,46]. The motion of the freed electron is calculated by solving Newton's equation of motion in one dimension for a static electric field $E(t) = E_{\text{peak}}$. Because the exact nonisotropic potential is usually not available in the experiment, we approximate the potential Eq. (1) in terms of a few parameters via the multipole expansion

$$\tilde{V}(\vec{r}; R, \theta) = -\frac{2}{r} + \frac{1}{2}\frac{\vec{r}^T \cdot \mathbf{Q}_{\text{L}}(R, \theta) \cdot \vec{r}}{r^5}, \quad (9)$$

where $\mathbf{Q}_{\text{L}} = \mathbf{M}^T \mathbf{Q} \mathbf{M}$, $\mathbf{M}(\theta)$ is a rotation matrix, and $\mathbf{Q}(R)$ is the quadrupole tensor in the molecular frame $\theta = 0$. Note that the dipole term of the potential Eq. (1) is zero and thus $V(\vec{r}) = \tilde{V}(\vec{r}) + O(r^{-4})$. By switching the potential off, one can determine the influence of the Coulomb tail on the trajectory after ionization. The attoclock shift is computed as $\Delta p_y = \lim_{t\to\infty}[p_{\tilde{V}=0}(t) - p_{\tilde{V}\neq 0}(t)]$. The orientation dependence of this result is mainly due to the Stark-shifted ionization potential, which enters the model only for calculating the exit point. Nevertheless, using a nonisotropic potential in the time-evolution step, instead of the isotropic approximation $-2/r$ applied in Ref. [37], we obtain a slightly better agreement with the TDSE.

Figure 3(a) shows our extrapolated TDSE results for HeH$^+$ (black solid line) in comparison to the two-step models with different exit points. The TBW approach (dash-dotted orange line) uses

$$y_0^{\text{TBW}} = -\frac{I_p(E)}{E}, \quad (10)$$

where $E > 0$ is the field strength at the ionization time, in our case always set to $E = E_{\text{peak}}$. The TBW leads to a severe underestimation of the attoclock shift in the adiabatic limit. This exit point is too large to provide enough momentum via the Coulomb attraction during the propagation. The FDM (dotted blue line) tunnel exit is defined by a numerical solution of

$$\tilde{V}(y_0^{\text{FDM}}) + y_0^{\text{FDM}}E = -I_p(E), \quad (11)$$

where $\tilde{V}$ is a cut through the potential Eq. (9) at $x = 0$. The FDM-based two-step model overestimates the attoclock shift in agreement with previous observations for helium [46]. An analytical solution of Eq. (11) (not plotted) can be obtained for $\tilde{V}(y_0) = -Z/|y_0|$, which changes the attoclock shift by less than about 10^{-3} a.u. compared to the numerical FDM. Here, Z is the charge of the residual molecular ion. The TIPIS model (dashed red line) uses the exit point

$$y_0^{\text{TIPIS}} = -\frac{I_p(E) + \sqrt{I_p(E)^2 - 4\beta_{2D}(E)E}}{2E}, \quad (12)$$

where $\beta_{2D} = Z - \frac{\sqrt{2I_p(E)}}{4}$, since the two-dimensional asymptotic ground-state wave function has no nodes [44,46,56]. This model predicts attoclock shifts slightly below the TDSE results.

TABLE I. Exact molecular parameters for the 2D HeH$^+$ molecule and parameters obtained by matching TIPIS- and FDM-based two-step models to TDSE results. The parameters are given in atomic units. Relative deviations are given in parentheses.

	$I_p(0)$	$\Delta\mu$	$\Delta\overline{\alpha}$	$\Delta\alpha_d$
Exact	1.657	0.4043	1.060	0.1944
TIPIS		0.4126 (2.1%)		0.2082 (7.1%)
FDM		0.3307 (18%)		0.3805 (95%)
TIPIS 2263 nm		0.4887 (21%)		0.01532 (92%)

In order to compare the different models, one can expand Eq. (12) in a series as

$$|y_0^{\text{TIPIS}}| = \frac{I_p(E)}{E}\left[1 - \frac{1}{2}\sum_{n=1}^{\infty}(-1)^{n-1}\binom{\frac{1}{2}}{n}\left(\frac{4\beta_{2D}E}{I_p(E)^2}\right)^n\right]. \quad (13)$$

In usual systems, e.g., atoms and small molecules at moderate field strength, the sum converges and causes a negative contribution to $|y_0^{\text{TIPIS}}|$, shifting the exit point towards the nuclei compared to the TBW. The analytical solution of the FDM is recovered when β_{2D} is replaced by Z. Since $0 < \beta_{2D} < Z$, the TIPIS exit point has a value between the FDM and the TBW.

The leading nonadiabatic correction to the exit point can be estimated in the strong-field approximation (SFA) for the given effective vector potential Eq. (4) as [57,58]

$$|y_0^{\text{nonadi.}}| \approx \frac{I_p}{E_{\text{peak}}}\left(1 - \frac{\gamma^2}{4} + O(\gamma^4)\right). \quad (14)$$

Here, the TBW is modified towards smaller values, too. While the SFA neglects the Coulomb interaction, we nevertheless expect that the reduction of the exit-point value is a general effect that plays a role for the attoclock shift in nonadiabatic conditions, i.e., finite wavelengths. This is consistent with Fig. 2(c) where the attoclock shifts are increased at small wavelengths. Agreement of the FDM-based attoclock shifts with TDSE solutions at finite wavelengths may therefore be accidental.

The remaining differences between the TDSE limit and the two-step models are on the order of 10^{-2} a.u. We checked numerical convergence by halving the time step and doubling the box lengths. Further, we choose a range of wavelengths for extrapolation where nonadiabatic effects are small ($\gamma \lesssim 0.28$), but also depletion does not disturb the attoclock shift (total ionization yield below 10^{-3}). Notice that a too large fitting range around the peak of the PMD induces a systematic error shifting the TDSE attoclock shifts to smaller values, artificially improving the agreement with the TIPIS model. We also compared the one-dimensional two-step models with two-dimensional models using the full time-dependent field instead of a static field. We find no difference in the adiabatic limit and see no indications of rescattering.

In the two-step models, we use the exact molecular parameters $I_p(0)$, $\Delta\mu$, $\Delta\overline{\alpha}$, and $\Delta\alpha_d$ for the 2D molecule (see Table I). These are extracted from the Stark shifts in a TDSE solution with a weak linearly increasing electric field [37]. In Fig. 3(b), we selectively set molecular parameters to zero
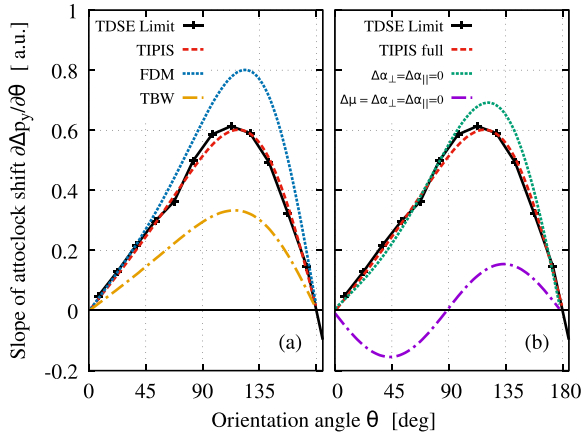
FIG. 4. Same as Fig. 3 except that the numerical derivative of the orientation-dependent attoclock shift is shown.

to see the influence of the quadratic and linear term of the Stark-shifted ionization potential, Eq. (8), in the TIPIS model. When neglecting the dipole moment and the polarizabilities (dash-dotted purple line), the ionization potential and thus the exit point become independent of the orientation. The remaining angle dependence of the attoclock shift results only from the propagation of the outgoing trajectory in the potential Eq. (9). When including the dipole moment $\Delta\mu$, we find that it is responsible for the pronounced monotonic trend from $0°$ to the maximum at $180°$ [see the dotted green line in Fig. 3(b)]. In contrast to the full TIPIS model (dashed red line), however, the results without polarizability are not parallel to the TDSE results. In particular, the difference between the maximal and minimal values is not well reproduced without polarizability.

The results indicate that the TIPIS model reproduces the attoclock shift very well except for an angle-independent offset. Therefore, we proceed to analyze the slope, i.e., the derivative of the attoclock shift with respect to the orientation angle. Figure 4 shows the numerical derivative of the data from Fig. 3. In Fig. 4(a), we see excellent agreement between the slope of the TIPIS-based model and the TDSE results. Further, the FDM and the TBW show a quantitatively wrong behavior. Figure 4(b) shows that the polarizabilities are necessary to form the correct slope. Based on this observation, we expect that the molecular properties can be extracted just from the slope. This approach has the additional advantage that it does not require the measurement of an absolute attoclock shift, but only the relative orientation dependence.

Extraction of molecular parameters. In the simulations, we optimize the parameters $\Delta\mu$ and $\Delta\alpha_d$, which influence the

orientation dependence most strongly, for best agreement of the TIPIS-based model with the slope of the TDSE results (Fig. 4), minimizing the mean squared error. We assume the total charge and the quadrupole moment $\mathbf{Q}$ in Eq. (9) to be given. The results are given in Table I. For the TIPIS model, the parameters can be reproduced within a relative deviation of 7% from the exact values. This shows that the slope of the orientation-dependent adiabatic attoclock shift can be understood and reproduced within a very simple model. In our system we cannot extract information about the ionic potential, i.e., the quadrupole tensor, because its effect on the attoclock shift is too similar to the effect of the quadratic term of the Stark-shifted ionization potential, so the fitting routine will not converge reliably. However, for a more complex functionality of the orientation-dependent attoclock shift, this may be possible. With the same optimization procedure, the FDM converges to poor results (molecular parameters up to 95% from the exact parameters). Finally, we attempt to extract molecular parameters from TDSE results at finite wavelengths, because such data are experimentally easier to obtain than the adiabatic limit. We expect that the TIPIS model cannot reproduce these curves accurately, and indeed we find errors up to 92% for the molecular parameters when matching the TIPIS results to the symmetrized TDSE results at 2263 nm.

Conclusions. To conclude, we have presented a scheme to extract molecular properties from the slope of the orientation-dependent adiabatic attoclock shift, which is obtained from PMDs at sufficiently long wavelengths of a quasilinear field. We have shown that a TIPIS-based two-step model reproduces these data with high accuracy, leading to a precise measurement of molecular properties. On the other hand, our results indicate that one cannot expect adiabatic models to be accurate at typical infrared wavelengths. This has to be considered when analyzing experiments. We have provided an expression for the effective frequency and the optimal ratio between the two circularly polarized components of the bicircular field to obtain the quasilinear field. It appears promising to combine the bicircular attoclock with a pump-probe scheme to track ultrafast changes during time-dependent processes with moving nuclei. Future work may also consider the effect of molecular chirality on the attoclock shifts considering the electric multipoles implied by a chiral structure.

[1] A. McPherson, G. Gibson, H. Jara, U. Johann, T. S. Luk, I. A. McIntyre, K. Boyer, and C. K. Rhodes, Studies of multiphoton production of vacuum-ultraviolet radiation in the rare gases, J. Opt. Soc. Am. B **4**, 595 (1987).

[2] T. Zuo, A. D. Bandrauk, and P. B. Corkum, Laser-induced electron diffraction: a new tool for probing ultrafast molecular dynamics, Chem. Phys. Lett. **259**, 313 (1996).

[3] M. Lein, J. P. Marangos, and P. L. Knight, Electron diffraction in above-threshold ionization of molecules, Phys. Rev. A **66**, 051404(R) (2002).

[4] M. Meckel, D. Comtois, D. Zeidler, A. Staudte, D. Pavičić, H. C. Bandulet, H. Pépin, J. C. Kieffer, R. Dörner, D. M. Villeneuve, and P. B. Corkum, Laser-induced electron tunneling and diffraction, Science **320**, 1478 (2008).

[5] C. I. Blaga, J. Xu, A. D. DiChiara, E. Sistrunk, K. Zhang, P. Agostini, T. A. Miller, L. F. DiMauro, and C. D. Lin, Imaging ultrafast molecular dynamics with laser-induced electron diffraction, Nature (London) **483**, 194 (2012).

[6] B. Belsa, K. M. Ziems, A. Sanchez, K. Chirvi, X. Liu, S. Gräfe, and J. Biegert, Laser-induced electron diffraction in the

over-the-barrier-ionization regime, Phys. Rev. A **106**, 043105 (2022).

[7] Y. Huismans, A. Rouzée, A. Gijsbertsen, J. H. Jungmann, A. S. Smolkowska, P. S. W. M. Logman, F. Lépine, C. Cauchy, S. Zamith, T. Marchenko, J. M. Bakker, G. Berden, B. Redlich, A. F. G. van der Meer, H. G. Muller, W. Vermin, K. J. Schafer, M. Spanner, M. Y. Ivanov, O. Smirnova *et al.*, Time-resolved holography with photoelectrons, Science **331**, 61 (2011).

[8] S. G. Walt, N. Bhargava Ram, M. Atala, N. I. Shvetsov-Shilovski, A. von Conta, D. Baykusheva, M. Lein, and H. J. Wörner, Dynamics of valence-shell electrons and nuclei probed by strong-field holography and rescattering, Nat. Commun. **8**, 15651 (2017).

[9] C. F. de Morisson Faria and A. S. Maxwell, It is all about phases: ultrafast holographic photoelectron imaging, Rep. Prog. Phys. **83**, 034401 (2020).

[10] T. K. Kjeldsen, C. Z. Bisgaard, L. B. Madsen, and H. Stapelfeldt, Role of symmetry in strong-field ionization of molecules, Phys. Rev. A **68**, 063407 (2003).

[11] T. K. Kjeldsen, C. Z. Bisgaard, L. B. Madsen, and H. Stapelfeldt, Influence of molecular symmetry on strong-field ionization: Studies on ethylene, benzene, fluorobenzene, and chlorofluorobenzene, Phys. Rev. A **71**, 013418 (2005).

[12] T. Brabec, M. Côté, P. Boulanger, and L. Ramunno, Theory of tunnel ionization in complex systems, Phys. Rev. Lett. **95**, 073001 (2005).

[13] L. Holmegaard, J. L. Hansen, L. Kalhøj, S. Louise Kragh, H. Stapelfeldt, F. Filsinger, J. Küpper, G. Meijer, D. Dimitrovski, M. Abu-samha, C. P. J. Martiny, and L. Bojer Madsen, Photoelectron angular distributions from strong-field ionization of oriented molecules, Nat. Phys. **6**, 428 (2010).

[14] D. Dimitrovski, C. P. J. Martiny, and L. B. Madsen, Strong-field ionization of polar molecules: Stark-shift-corrected strong-field approximation, Phys. Rev. A **82**, 053404 (2010).

[15] D. Dimitrovski, M. Abu-samha, L. B. Madsen, F. Filsinger, G. Meijer, J. Küpper, L. Holmegaard, L. Kalhøj, J. H. Nielsen, and H. Stapelfeldt, Ionization of oriented carbonyl sulfide molecules by intense circularly polarized laser pulses, Phys. Rev. A **83**, 023405 (2011).

[16] J. L. Hansen, L. Holmegaard, L. Kalhøj, S. L. Kragh, H. Stapelfeldt, F. Filsinger, G. Meijer, J. Küpper, D. Dimitrovski, M. Abu-samha, C. P. J. Martiny, and L. B. Madsen, Ionization of one- and three-dimensionally-oriented asymmetric-top molecules by intense circularly polarized femtosecond laser pulses, Phys. Rev. A **83**, 023406 (2011).

[17] L. V. Keldysh, Ionization in the field of a strong electromagnetic wave, Sov. Phys. JETP **20**, 1307 (1965).

[18] P. Eckle, M. Smolarski, P. Schlup, J. Biegert, A. Staudte, M. Schöffler, H. G. Muller, R. Dörner, and U. Keller, Attosecond angular streaking, Nat. Phys. **4**, 565 (2008).

[19] P. Eckle, A. N. Pfeiffer, C. Cirelli, A. Staudte, R. Dörner, H. G. Muller, M. Büttiker, and U. Keller, Attosecond ionization and tunneling delay time measurements in helium, Science **322**, 1525 (2008).

[20] U. S. Sainadh, H. Xu, X. Wang, A. Atia-Tul-Noor, W. C. Wallace, N. Douguet, A. Bray, I. Ivanov, K. Bartschat, A. Kheifets *et al.*, Attosecond angular streaking and tunnelling time in atomic hydrogen, Nature (London) **568**, 75 (2019).

[21] R. Boge, C. Cirelli, A. S. Landsman, S. Heuser, A. Ludwig, J. Maurer, M. Weger, L. Gallmann, and U. Keller, Probing

nonadiabatic effects in strong-field tunnel ionization, Phys. Rev. Lett. **111**, 103003 (2013).

[22] V. V. Serov, A. W. Bray, and A. S. Kheifets, Numerical attoclock on atomic and molecular hydrogen, Phys. Rev. A **99**, 063428 (2019).

[23] K. Fehre, S. Eckart, M. Kunitski, C. Janke, D. Trabert, J. Rist, M. Weller, A. Hartung, M. Pitzer, L. P. H. Schmidt *et al.*, Angular streaking in strong field ionization of chiral molecules, Phys. Rev. Res. **1**, 033045 (2019).

[24] W. Quan, V. V. Serov, M. Z. Wei, M. Zhao, Y. Zhou, Y. L. Wang, X. Y. Lai, A. S. Kheifets, and X. J. Liu, Attosecond molecular angular streaking with all-ionic fragments detection, Phys. Rev. Lett. **123**, 223204 (2019).

[25] A. S. Kheifets, The attoclock and the tunneling time debate, J. Phys. B: At. Mol. Opt. Phys. **53**, 072001 (2020).

[26] J. Yan, W. Xie, M. Li, K. Liu, S. Luo, C. Cao, K. Guo, W. Cao, P. Lan, Q. Zhang, Y. Zhou, and P. Lu, Photoelectron ionization time of aligned molecules clocked by attosecond angular streaking, Phys. Rev. A **102**, 013117 (2020).

[27] A. Khan, D. Trabert, S. Eckart, M. Kunitski, T. Jahnke, and R. Dörner, Orientation-dependent dissociative ionization of H_2 in strong elliptic laser fields: Modification of the release time through molecular orientation, Phys. Rev. A **101**, 023409 (2020).

[28] D. Trabert, S. Brennecke, K. Fehre, N. Anders, A. Geyer, S. Grundmann, M. S. Schöffler, L. P. H. Schmidt, T. Jahnke, R. Dörner *et al.*, Angular dependence of the Wigner time delay upon tunnel ionization of H_2, Nat. Commun. **12**, 1697 (2021).

[29] D. Trabert, N. Anders, A. Geyer, M. Hofmann, M. Schöffler, L. P. H. Schmidt, T. Jahnke, M. Kunitski, R. Dörner, and S. Eckart, Angular dependence of the Wigner time delay upon strong-field ionization from an aligned *p* orbital, Phys. Rev. Res. **5**, 023118 (2023).

[30] A. Geyer, D. Trabert, M. Hofmann, N. Anders, M. Schöffler, L. P. H. Schmidt, T. Jahnke, M. Kunitski, R. Dörner, and S. Eckart, Experimental fingerprint of the electron's longitudinal momentum at the tunnel exit in strong field ionization, Phys. Rev. Res. **5**, 033094 (2023).

[31] M. Paul, L. Yue, and S. Gräfe, Imprints of the molecular electronic structure in the photoelectron spectra of strong-field ionized asymmetric triatomic model molecules, Phys. Rev. Lett. **120**, 233202 (2018).

[32] M. Yu, K. Liu, M. Li, J. Yan, C. Cao, J. Tan, J. Liang, K. Guo, W. Cao, P. Lan *et al.*, Full experimental determination of tunneling time with attosecond-scale streaking method, Light Sci. Appl. **11**, 215 (2022).

[33] S. Brennecke, S. Eckart, and M. Lein, Attoclock with bicircular laser fields as a probe of velocity-dependent tunnel-exit positions, J. Phys. B: At., Mol. Opt. Phys. **54**, 164001 (2021).

[34] S. Eckart, M. Kunitski, I. Ivanov, M. Richter, K. Fehre, A. Hartung, J. Rist, K. Henrichs, D. Trabert, N. Schlott, L. P. H. Schmidt, T. Jahnke, M. S. Schöffler, A. Kheifets, and R. Dörner, Subcycle interference upon tunnel ionization by counter-rotating two-color fields, Phys. Rev. A **97**, 041402(R) (2018).

[35] S. Eckart, K. Fehre, N. Eicke, A. Hartung, J. Rist, D. Trabert, N. Strenger, A. Pier, L. P. H. Schmidt, T. Jahnke, M. S. Schöffler, M. Lein, M. Kunitski, and R. Dörner, Direct experimental access to the nonadiabatic initial momentum offset upon tunnel ionization, Phys. Rev. Lett. **121**, 163202 (2018).

[36] N. Eicke and M. Lein, Attoclock with counter-rotating bicircular laser fields, Phys. Rev. A **99**, 031402(R) (2019).

[37] N. Eicke, S. Brennecke, and M. Lein, Attosecond-scale streaking methods for strong-field ionization by tailored fields, Phys. Rev. Lett. **124**, 043202 (2020).

[38] H. Eichmann, A. Egbert, S. Nolte, C. Momma, B. Wellegehausen, W. Becker, S. Long, and J. K. McIver, Polarization-dependent high-order two-color mixing, Phys. Rev. A **51**, R3414 (1995).

[39] O. Kfir, P. Grychtol, E. Turgut, R. Knut, D. Zusin, D. Popmintchev, T. Popmintchev, H. Nembach, J. M. Shaw, A. Fleischer, H. Kapteyn, M. Murnane, and O. Cohen, Generation of bright phase-matched circularly-polarized extreme ultraviolet high harmonics, Nat. Photon. **9**, 99 (2015).

[40] D. B. Milošević and W. Becker, Improved strong-field approximation and quantum-orbit theory: Application to ionization by a bicircular laser field, Phys. Rev. A **93**, 063418 (2016).

[41] M. Abu-samha and L. B. Madsen, Probing atomic and molecular targets by intense bicircular counter-rotating laser fields, J. Phys. B: At., Mol. Opt. Phys. **51**, 135401 (2018).

[42] D. Habibović, A. Čerkić, M. Busuladžić, A. Gazibegović-Busuladžić, S. Odžak, E. Hasović, and D. B. Milošević, Molecules in a bicircular strong laser field, Opt. Quantum Electron. **50**, 214 (2018).

[43] N. B. Delone and V. P. Krainov, Energy and angular electron spectra for the tunnel ionization of atoms by strong low-frequency radiation, J. Opt. Soc. Am. B **8**, 1207 (1991).

[44] H. Ni, N. Eicke, C. Ruiz, J. Cai, F. Oppermann, N. I. Shvetsov-Shilovski, and L.-W. Pi, Tunneling criteria and a nonadiabatic term for strong-field ionization, Phys. Rev. A **98**, 013411 (2018).

[45] P. B. Corkum, N. H. Burnett, and F. Brunel, Above-threshold ionization in the long-wavelength limit, Phys. Rev. Lett. **62**, 1259 (1989).

[46] A. N. Pfeiffer, C. Cirelli, M. Smolarski, D. Dimitrovski, M. Abu-samha, L. B. Madsen, and U. Keller, Attoclock reveals natural coordinates of the laser-induced tunnelling current flow in atoms, Nat. Phys. **8**, 76 (2012).

[47] D. Dimitrovski and L. B. Madsen, Theory of low-energy photoelectrons in strong-field ionization by laser pulses with large ellipticity, Phys. Rev. A **91**, 033409 (2015).

[48] T. Brabec, M. Y. Ivanov, and P. B. Corkum, Coulomb focusing in intense field atomic processes, Phys. Rev. A **54**, R2551 (1996).

[49] M. D. Feit, J. A. Fleck, Jr., and A. Steiger, Solution of the Schrödinger equation by a spectral method, J. Comput. Phys. **47**, 412 (1982).

[50] R. Kosloff and H. Tal-Ezer, A direct relaxation method for calculating eigenfunctions and eigenvalues of the Schrödinger equation on a grid, Chem. Phys. Lett. **127**, 223 (1986).

[51] F. Oppermann, N. Eicke, and M. Lein, Real-time propagator eigenstates, J. Phys. B: At., Mol. Opt. Phys. **55**, 19LT01 (2022).

[52] M. Lein, E. K. U. Gross, and V. Engel, Intense-field double ionization of helium: Identifying the mechanism, Phys. Rev. Lett. **85**, 4707 (2000).

[53] A. Ludwig, J. Maurer, B. W. Mayer, C. R. Phillips, L. Gallmann, and U. Keller, Breakdown of the dipole approximation in strong-field ionization, Phys. Rev. Lett. **113**, 243001 (2014).

[54] S. Brennecke, Electron momentum distributions from strong-field-induced ionization of atoms and molecules, Ph.D. thesis, Gottfried Willhelm Leibniz University, Hannover, 2023.

[55] S. Brennecke, N. Eicke, and M. Lein, Gouy's phase anomaly in electron waves produced by strong-field ionization, Phys. Rev. Lett. **124**, 153202 (2020).

[56] N. I. Shvetsov-Shilovski, D. Dimitrovski, and L. B. Madsen, Ionization in elliptically polarized pulses: Multielectron polarization effects and asymmetry of photoelectron momentum distributions, Phys. Rev. A **85**, 023428 (2012).

[57] A. M. Perelomov, V. S. Popov, and M. V. Terent'ev, Ionization of atoms in an alternating electric field: II, Sov. Phys. JETP **24**, 207 (1967).

[58] M. Li, J.-W. Geng, M. Han, M.-M. Liu, L.-Y. Peng, Q. Gong, and Y. Liu, Subcycle nonadiabatic strong-field tunneling ionization, Phys. Rev. A **93**, 013402 (2016).